Biochemistry and Biophysics Reports 36 (2023) 101575

Contents lists available at ScienceDirect

Biochemistry and Biophysics Reports

journal homepage: www.elsevier.com/locate/bbrep

# Utility of ultrasonography in a mouse model of non-alcoholic steatohepatitis induced by a choline-deficient, high-fat diet and dextran sulfate sodium

Fuki Hayakawa [a], Koichi Soga [a], Junko Fujino [b], Takahiro Ota [a], Mayumi Yamaguchi [a], Masaya Tamano [a,*]

[a] Department of Gastroenterology, Dokkyo Medical University Saitama Medical Center, 2-1-50 Minami-Koshigaya, Koshigaya-shi, Saitama, 343-8555, Japan
[b] Department of Surgery, Division of Pediatric Surgery, Iwate Medical University, 1-1-3 Idaidori, Yahaba-cho, Shiwa-gun, Iwate, 028-3694, Japan

ARTICLE INFO

*Keywords:*
Animal experimentation
Colitis
Fatty liver
Hepatitis
Tumorigenesis
Ultrasonography

ABSTRACT

*Background:* Nonalcoholic steatohepatitis (NASH) is a chronic progressive liver disease that can progress to cirrhosis and hepatocellular carcinoma. The prevalence of NASH is increasing year by year. However, the etiology and progression of NASH, along with the processes leading to carcinogenesis, remain poorly understood. A range of animal models are used in research, but investigators have been unable to establish a model that results in tumorigenesis from a stable disease state. The present study aimed to create a stable, low-mortality model of NASH using abdominal ultrasonography (US) to assess NASH stage and diagnose liver tumors.

*Methods:* Thirty-four 19-week-old male C57BL/6J mice were fed a choline-deficient, high-fat (CDHF) diet. Twenty animals were given seven courses of 0.8 % dextran sulfate sodium (DSS) for 7 days followed by 10 days of MilliQ water (CDHF+DSS group). The remaining 14 animals drank only MilliQ water (CDHF group). All animals were weighed weekly and US was performed on Days 35 and 120. After necropsy, samples were taken for biochemical analysis and histopathological evaluation.

*Results:* The CDHF+DSS group had significantly lower body weight on Days 35 and 120, and significantly higher liver/body weight (%) on Day 35 compared to the CDHF group. US on Days 35 and 120 revealed significantly shorter long intestine and higher colonic histological score in the CDHF+DSS group compared to the CDHF group. IL-1β and IL-6 levels in the large intestinal tissue were significantly higher in the CDHF+DSS group.

*Conclusions:* A stable, low-mortality model of NASH was created with a CDHF diet and intermittent 0.8 % DSS. Abdominal US can assess the degree of fatty degeneration and evaluate liver tumorigenesis without necropsy. This assessment procedure will reduce the number of mice killed unnecessarily during experiments, thereby contributing to animal welfare.

## 1. Introduction

Nonalcoholic steatohepatitis (NASH) is a type of nonalcoholic fatty liver disease (NAFLD) that is a chronic progressive liver disease characterized by fatty deposition in hepatocytes, as well as inflammatory cell invasion and balloon-like degeneration and fibrosis of hepatocytes. NASH can progress to hepatic cirrhosis and hepatocellular carcinoma. When NASH develops into cirrhosis, the spleen is enlarged and gets heavy. The colon lesion of NASH does not have the constant tendency but the change of the intestinal bacterial flora and increased intestinal permeability are regarded as important [1]. Conditions including metabolic syndrome and obesity are causing a worldwide increase in NAFLD [2]. The prevalence of NAFLD in Japan was 25 % in 2004, increased to 30 % in 2012, and is predicted to reach 45 % in 2040 [3]. NASH accounts for around 10 %–20 % of NAFLD cases, and this percentage presumably increases with increasing NAFLD prevalence [2].

The proportion of NASH that develops into cancer has increased recently [4]. The etiology and progression of NASH, along with the processes leading to carcinogenesis, remain poorly understood. A range of animal models are used in research, but investigators have been unable to establish a model that results in tumorigenesis from a stable disease state.

* Corresponding author.
*E-mail address:* mstamano@dokkyomed.ac.jp (M. Tamano).

https://doi.org/10.1016/j.bbrep.2023.101575
Received 9 August 2023; Received in revised form 30 October 2023; Accepted 31 October 2023
Available online 8 November 2023

Moreover, the assessment of liver tumors in mouse models requires necropsy with direct visual observation and microscopy. Instances in which no liver tumors are found on necropsy or the animal dies of illness before necropsy therefore directly reduce research efficiency. The availability of a mouse model in which liver tumors could be assessed without necropsy would increase research efficiency in this field. Moreover, the ability to assess liver tumors with the animals alive would allow observation of tumors over time and, thus, determination of the mode of tumor progression, as well as the rate of tumor growth, which would in turn contribute to research on tumor malignancy. From an animal welfare perspective, using abdominal ultrasonography (US) to assess model mice would reduce the number of animals that have to be killed unnecessarily.

Abdominal US is commonly used in clinical settings to diagnose NAFLD and identify liver tumors. Detailed observations and elastography in B-mode allow NAFLD to be staged [5–7].

The present study had two objectives. One was to create a stable model of NASH with few deaths occurring during the observation phase. The other was to determine whether US could be used in this model to assess NASH stage and diagnose liver tumors.

## 2. Materials and methods

### 2.1. Animals and treatment

Thirty-four 19-week-old male C57BL/6J mice purchased from SLC Japan (Shizuoka, Japan) were acclimated for 7 days. During acclimation, the animals were given MilliQ water to drink and fed a standard diet of CLEA Rodent Diet CE-2 (A06071302) (CLEA Japan, Tokyo). The animals were reared in an environment with one animal per cage, a 12-h light-dark cycle controlled to a temperature of 18 °C to 26 °C and humidity of 30 %–60 %. On Day 1, which was 8 days after purchase, all mice were switched to a choline-deficient, high-fat diet (CDHF) (Research Diets Inc., USA). The 34 animals were divided into two groups. Twenty animals were given 0.8 % dextran sulfate sodium (DSS) to drink for 7 days, followed by MilliQ water for the next 10 days; this represented one course of treatment. The animals were given up to 7 courses according to a similar schedule (CDHF+DSS group). The remaining 14 animals were given only MilliQ water to drink (CDHF group).

All animals were weighed weekly during the study. The animals in each group underwent US on Days 35 and 120 and were subsequently necropsied. Blood was used for biochemical analysis, and the liver, spleen, and large colon were processed for histopathological evaluation.

The procedures used for the handling and care of animals were approved by the Animal Experiment Committee, Dokkyo Medical University (approved No. 1430), and conformed to the national guidelines for animal usage in research.

### 2.2. Ultrasonography

The LOGIQ e Premium was used as the ultrasound machine with an L10-22RS probe (both by GE Healthcare, Tokyo, Japan). The machine was configured to have a depth of field of 1.5 cm, focus at 3 points (0.2, 0.5, and 1.0 cm), and gain of 51 dB. US was performed with the animals anesthetized by an intraperitoneal injection of a 3-drug combination anesthetic (medetomidine, midazolam, and butorphanol at 0.3, 4.0, and 5.0 mg/kg, respectively). The entire abdomen of the mice was shaved, and the animals were immobilized in a supine position. We performed the observation in midline vertical scanning (A), right side vertical span scanning (B) and right rib arch bottom scanning (C). Hepatorenal echo contrast (HEC) was evaluated in scan (B) and heterogeneity of liver parenchyma (HOLP) was evaluated in scan (A) and (C). And then, the whole liver was performed for confirming the presence or absence of liver tumor.

The image analysis program WinROOF2021 (Mitani Corporation, Tokyo, Japan) was used to evaluate ultrasound images. Identically sized regions of interest (ROIs) were set in the images of the liver and kidneys acquired with vertical scanning. Concentration characteristics were measured, and brightness was quantified. The ratio of liver to kidney brightness was defined as the HEC ratio and used as a measure of fatty change. ROIs were set on the images of the liver acquired with horizontal scanning. Concentration characteristics were measured, and the standard deviation of brightness was calculated and defined as the HOLP index, which was used as a measure of liver fibrosis.

### 2.3. General tissue preparation

After US, blood was collected from the inferior vena cava. The animals were then euthanized by exsanguination and necropsied. The liver, spleen, and large colon were collected. The liver and spleen were weighed, and the length of the colon was determined. These organs were then fixed in 10 % neutral buffered formalin. A portion of the left lateral lobe of the liver was preserved in RNAlater (ThermoFisher, Tokyo, Japan). Serum was obtained by centrifuging the blood at 3000 $\times g$ for 15 min [8].

### 2.4. Biochemical analysis

Blood levels of aspartate transaminase (AST) and alanine aminotransferase (ALT) were determined. Analysis was performed with the DRI-CHEM NX700V (FUJIFILM, Tokyo, Japan).

### 2.5. Histology and immunohistochemistry

The livers and colons removed from the mice in each group were fixed in 10 % neutral buffered formalin and embedded in paraffin. Hepatic sections were cut from paraffin blocks for staining with hematoxylin and eosin (H&E) and Picro-Sirius Red Stain kit (ScyTek Laboratories Inc., USA) (3-μm thick) for histological examination. Colonic sections were cut for staining with H&E (7-μm thick) for histological examination. For immunohistochemistry, samples were incubated overnight with anti-F4/80 antibody (A700-209, 1:500, Bethyl Laboratories America, USA), followed by incubation with Histofine Simple Stain Mouse MAX-PO (Rabbit) (Nichirei, Japan) for 2 h. Antigen retrieval was performed by heating at 121 °C for 5 min in an autoclave with citrate buffer at pH 6.0 [8].

The program WinROOF2021 was used to measure regions of fatty deposition, sirius red-positive regions, and F4/80-positive regions. The color of the objective region of specimens was made the 2 level, and area differences and other regions were compared. Blood vessel areas and vessel wall portions were excluded from the calculations.

The colon was scored histologically according to the following previously reported scoring procedures: focally increased numbers of inflammatory cells in the lamina propria were scored as 1, confluence of inflammatory cells extending into the submucosa as 2, and transmural extension of the infiltrate as 3.

For tissue damage, discrete lymphoepithelial lesions were scored as 1, mucosal erosions as 2, and extensive mucosal damage and/or extension through deeper structures of the bowel wall as 3.

The two equally weighted subscores (cell infiltration and tissue damage) were added, and the combined histological colitis severity score ranged from 0 to 6 [9].

### 2.6. RNA extraction and quantitative RNA analysis

Total RNA was extracted from tissues of the left lateral lobe of the liver saved in RNAlater using ISOGEN (NIPPON GENE CO., Japan). Total RNA was isolated using the QuantiTect Reverse Transcription Kit (Qiagen, Germany) (Cat: 205313) including an RNase-free DNAse step, and mRNA was quantified using the QuantStudio 5 real-time PCR system. TaqMan probes (IL1-β, α-SMA)(ThermoFisher Scientific) (Gen-ID:

**Table 1**
CDHF + DSS-induced liver injury in mice.

| | Day 35 | | | Day 120 | | |
|---|---|---|---|---|---|---|
| | CDHF (n = 7) | CDHF+DSS (n = 10) | *p* value | CDHF (n = 7) | CDHF+DSS (n = 10) | *p* value |
| Body weight (g) | 28.22±0.44 | 26.05±0.40 | 0.0019 | 31.14±0.71 | 24.92±0.89 | 0.0005 |
| Liver/Body weight (%) | 7.86±0.54 | 7.98±1.97 | 0.8453 | 8.39±0.55 | 9.68±0.31 | 0.0166 |
| Spleen/Body weight (%) | 0.77±0.05 | 0.53±0.09 | 0.5658 | 0.65±0.03 | 0.49±0.09 | 0.1162 |
| Colonic length (cm) | 7.93±0.16 | 6.83±0.19 | 0.0028 | 8.01±0.12 | 6.52±0.16 | 0.0003 |
| Colonic histological score | 0.43±0.13 | 1.55±0.16 | 0.0008 | 0.56±0.22 | 2.00±0.23 | 0.0016 |
| AST (IU/L) | 269.5±19.7 | 470.4±42.5 | 0.0025 | 381.0±21.2 | 383.3±17.0 | 0.9433 |
| ALT (IU/L) | 278.6±32.3 | 683.7±70.9 | 0.0034 | 535.0±20.6 | 593.7±33.1 | 0.3277 |

Data are mean ± SEM.
ALT, alanine aminotransferase; ALT, aspartate aminotransferase.

Mm00434228, Mm1546133), Housekeeping Genes (Gapdh) (Applied Biosystems, USA), and TaqPath qPCR Master Mix, CG (Applied Biosystems) (Cat: A16245) were used for quantification.

### 2.7. Method for cytokine measurement in colon tissue

Excise a 2 cm segment of the colon and immediately flash-freeze it. Subsequently, store the tissue at −80 °C. Prepare tissue extraction solution by adding a protease inhibitor (Thermo Scientific)(Cat: A32955) to RIPAbuffer (containing 50 mM Tris-HCl(pH7.6), 150 mM NaCl, 0.5% Sodium deoxycholate, and 1%TritonX-100). Homogenize the colon tissue using the tissue extraction solution.Utilize this liquid as samples for ELISA. Measure IL-1β and IL-6 (Invitorogen)(Cat: BMS6002, BMS 603) using the ELISA method.

### 2.8. Correspondence of Ultrasound Findings to Histopathological Findings

The correlation of the HEC ratio (a measure of fatty change determined by US) to regions of fatty deposition identified on histological evaluation was investigated. The correlation of the HOLP index (a measure of fibrosis determined with US) to sirius red-positive regions was similarly investigated. For these investigations, the data were combined with the data from 8 healthy mice acquired in a previous study. In other words, the correlation were considered in 48 mice; 20 CHDF group, 20 CHDF+DSS group, 8 healthy group. Finally, ultrasound visualization of histologically confirmed liver tumors was investigated.

### 2.9. Statistical analysis

Continuous data are expressed as means ± standard error of mean

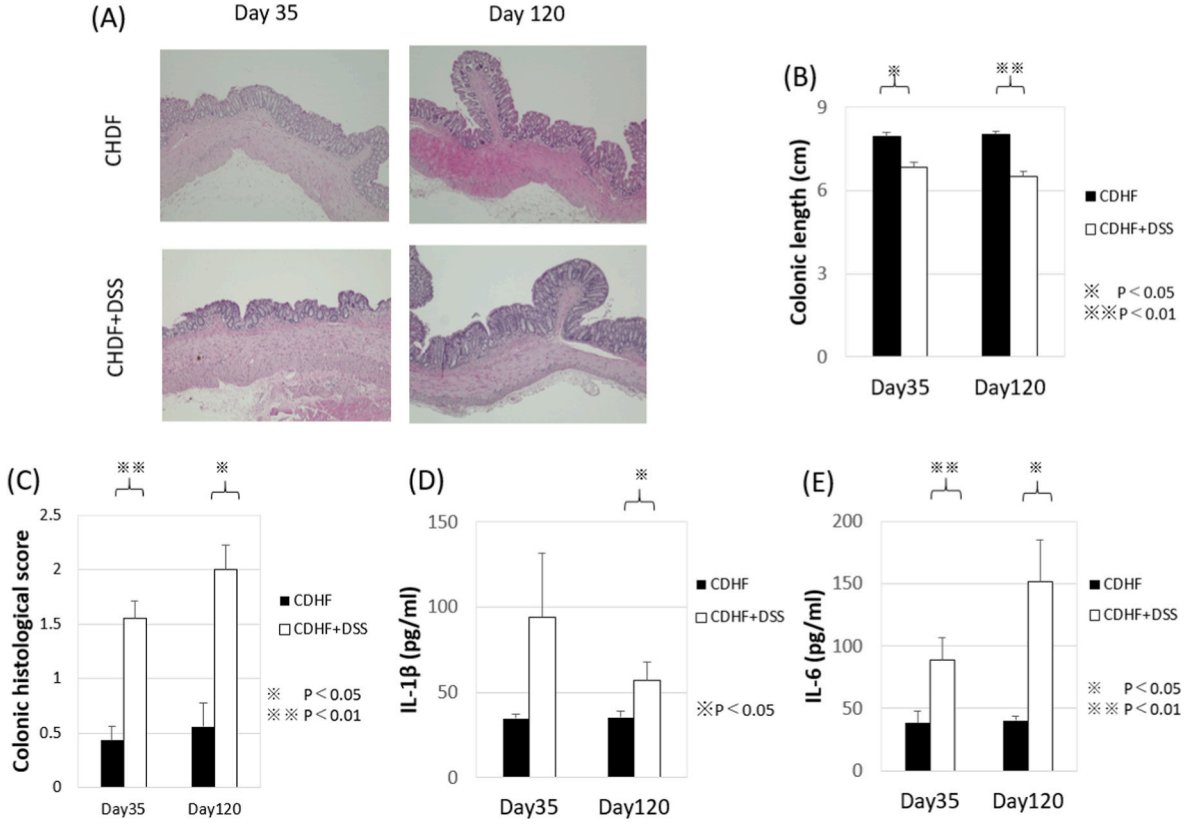


**Fig. 1.** Intestinal inflammation after DSS administration
A: Histopathological images of large intestinal samples from necropsy on Days 35 and 120 (hematoxylin and eosin (H&E), × 40). Findings of inflammatory cell invasion and mucosal damage are seen in the choline-deficient, high-fat diet (CDHF) + 0.8 % dextran sulfate sodium (DSS) group. B: Mean colonic length in the 2 groups at Days 35 and 120. Colonic length is significantly shorter in the CDHF+DSS group than in the CDHF group. C: Mean colonic histological score on Days 35 and 120. The score is significantly higher in the CDHF+DSS group than in the CDHF group. D and E: Mean levels of IL-1β and IL-6 from large intestinal tissue on Days 35 and 120. Levels of IL-1β on Day 120 and IL-6 on Days 35 and 120 are significantly higher in the CDHF+DSS group.

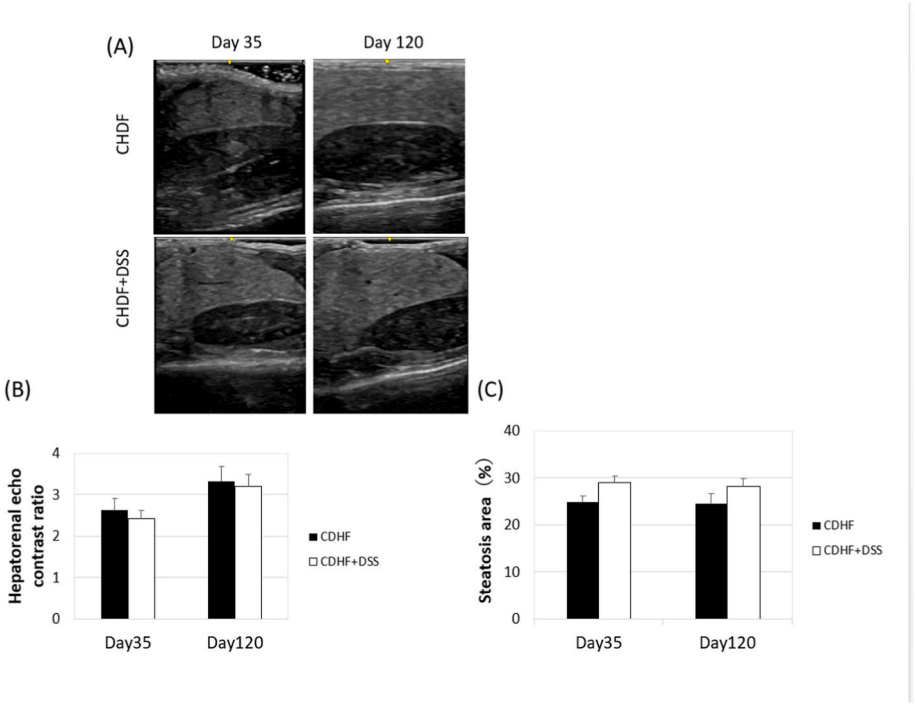


**Fig. 2.** Hepatic steatosis after DSS and CDHF diet administration
A: Abdominal ultrasound images of the liver on Days 35 and 120. In both the CDHF group and CDHF+DSS group, liver-kidney contrast is already positive on Day 35, with diagnostic imaging showing findings of hepatic steatosis. B: Mean values of the hepatorenal echo contrast ratio on Days 35 and 120. The values are elevated in both groups, but there is no significant between-group difference. C: Mean steatosis area on Days 35 and 120. The values are higher in the CDHF+DSS group, but there is no significant between-group difference.

(SEM). The Mann–Whitney test was used to compare the parameters of the CDHF group and the CDHF+DSS group on Days 35 and 120. Spearman's rank-correlation coefficient was used to test the correlations between ultrasound findings and histological findings. Correlation coefficients of 0.3 and greater were considered to indicate a correlation. In all statistical tests, a *P* value less than 0.05 was considered to indicate a significant difference.

## 3. Results

### 3.1. Body weight, liver to body weight, and spleen to body weight after DSS and CDHF diet administration

On Days 35, body weight was 28.22 g in CDHF+DSS group and 26.05 g in CDHF group ($p = 0.0019$). On Day 120, it was 31.14 g in CDHF+DSS group and 24.92 g in CDHF group ($p = 0.0005$). Liver/body weight (%) did not differ between the groups on Day 35, but it was significantly higher in the CDHF+DSS group on Day 120 (8.39 % vs 9.68 %, $p = 0.0166$). Spleen/body weight (%) did not differ between the groups on either Day 35 or Day 120 (Table 1).

### 3.2. Intestinal inflammation after DSS administration

Histological changes were seen in the colon in both groups. DSS exposure exacerbated histological findings such as crypt loss and increased inflammatory cells in the colon (Fig. 1A). On Days 35 and 120, the length of the colon was significantly shorter in the CDHF+DSS group than in the CDHF group (7.93 cm vs 6.83 cm, $p = 0.0028$ in Day 35 and 8.01 cm vs 6.52 cm, $p = 0.0003$ in Day 120) (Fig. 1B). On Days 35 and 120, the colonic histological score was significantly higher in the CDHF+DSS group than in the CDHF group (0.43 vs 1.55, $p = 0.0008$ in Day 35 and 0.53 vs 2.00, $p = 0.0003$ in Day 120) (Fig. 1C). Levels of IL-1β in the large intestinal tissue were significantly higher in the CDHF+DSS group (34.61 pg/ml vs 93.81 pg/ml, $p = 0.0907$ in Day 35 and 35.38 pg/ml vs 57.18 pg/ml, $p = 0.0475$ in Day 120) (Fig. 1D). Similarly, levels of IL-6 were significantly higher in the CDHF+DSS group (38.39 pg/ml vs 88.81 pg/ml, $p = 0.0312$ in Day 35 and 40.13 pg/ml vs 152.04 pg/ml, $p = 0.0263$ in Day 120) (Fig. 1E).

### 3.3. Hepatic steatosis after DSS and CDHF diet administration

Fig. 2A shows ultrasound scans on Days 35 and 120. In both groups, liver-kidney contrast was already positive on Day 35, with diagnostic imaging showing findings of hepatic steatosis. And there were no differences in ultrasonography findings between Day35 and Day120. In other words, steatosis of the liver was completed in early stage and it was maintained similar for a long term.

The HEC ratio did not differ between the groups on either Day 35 or Day 120 (Fig. 2B). On Days 35 and 120, the steatosis area was greater in the CDHF+DSS group, but not significantly (Fig. 2C).

### 3.4. Administration of DSS enhances CDHF diet-induced liver damage and inflamma11tion

Serum AST and ALT were significantly higher in the CDHF+DSS group on Day 35 (269.5 IU/L vs 470.4 IU/L, $p = 0.0025$ in AST and 278.6 IU/L vs 683.7 IU/L, $p = 0.0034$ in ALT). On Day 120, neither AST nor ALT differed significantly between the groups (Table 1). H&E stain was used to evaluate the level of fattiness and inflammation in the liver parenchyma. On Day 35, fatty deposition was increased in both groups, with no inter-group difference. Levels on Day 35 were comparable to those on Day 120. Many inflammatory cell infiltrations were observed in the CDHF+DSS group (Fig. 3A). The CDHF+DSS group also had increased expression of IL-1β associated with liver injury and inflammation (0.70 pg/ml vs 1.92 pg/ml, $p = 0.0082$) (Fig. 3B).

Tissue samples were stained with F4/80 immunohistochemical stain, which indicates inflammatory macrophage activation (Fig. 3C). In the CDHF+DSS group, F4/80-positive regions tended to be increased on Day

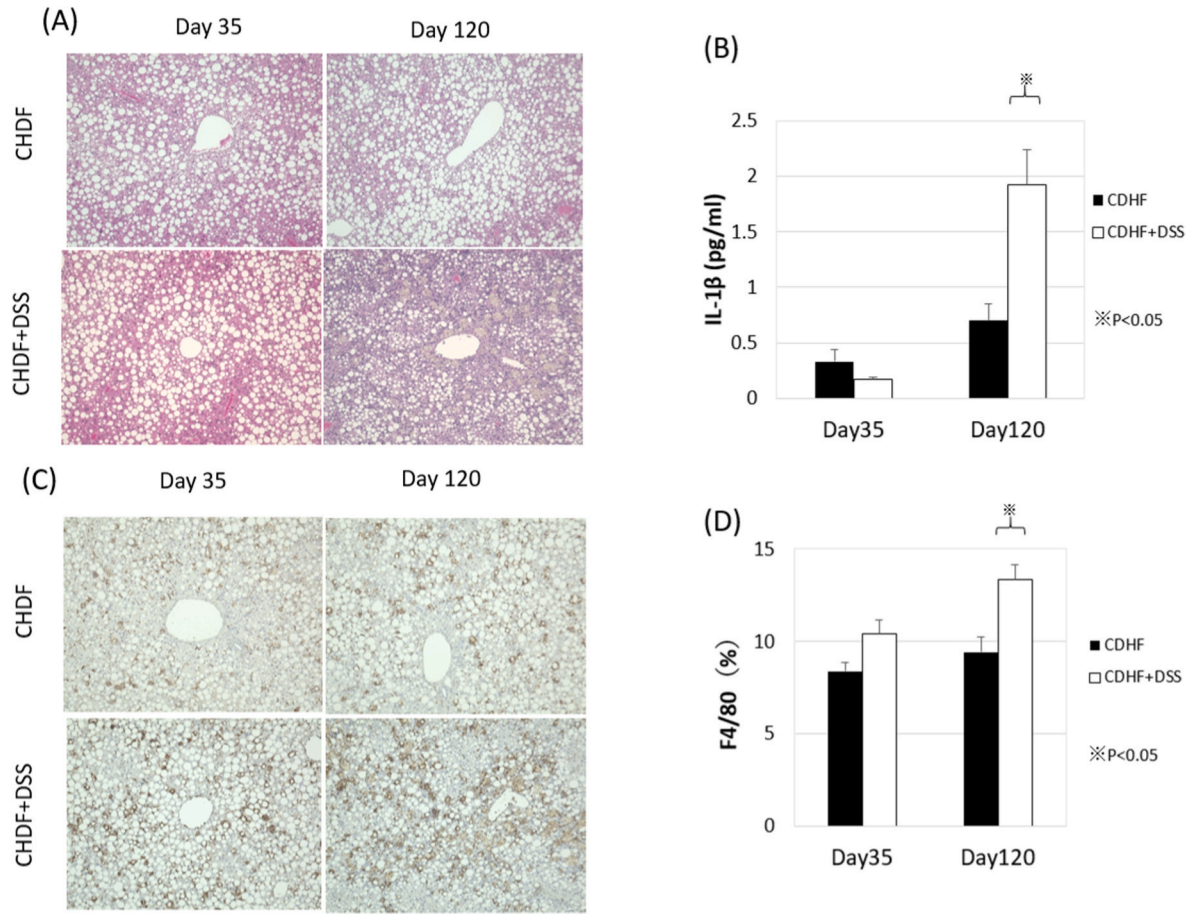


**Fig. 3.** Administration of DSS enhances CDHF diet-induced liver damage and inflammation
A: H&E-stained histopathological images of liver sampled at necropsy on Days 35 and 120 ( × 100). On Day 35, fatty deposition is increased in both groups, with no inter-group difference. Levels on Day 35 are comparable to those on Day 120. Many inflammatory cell infiltrations are seen in the CDHF+DSS group. B: Mean levels of IL-1β from liver tissue on Days 35 and 120. There is no between-group difference on Day 35, but the level is significantly higher in the CDHF+DSS group on Day 120. C: F4/80 immunohistologically stained images of liver sampled as in Fig. 3A ( × 100). F4/80-positive areas are stained brown. In the CDHF+DSS group, F4/80-positive regions tend to be increased on Day 35 and are significantly increased on Day 120 (Fig. 3D). (For interpretation of the references to color in this figure legend, the reader is referred to the Web version of this article.)

35 and were significantly increased on Day 120 (9.42 % vs 13.34 %, $p = 0.0079$) (Fig. 3D).

### 3.5. Administration of DSS promoted CDHF diet-induced hepatic fibrosis

Hepatic fibrosis was evaluated with sirius red stain (Fig. 4A). Although the sirius red-positive area did not differ between the groups on Day 35, it was significantly larger in the CDHF+DSS group on Day 120 (5.24 % vs 11.42 %, $p = 0.0209$) (Fig. 4B). The marker α-SMA, which is associated with liver fibrosis, similarly did not differ between the groups on Day 35, but it was significantly higher in the CDHF+DSS group on Day 120 (1.73 pg/ml vs 2.63 pg/ml, $p = 0.0132$) (Fig. 4C).

The HOLP index did not differ between the groups on Day 35, but it was higher in the CDHF+DSS group on Day 120, although in each group, the level on Day 120 was lower than on Day 35 (11.82 vs 13.78, $p = 0.0755$) (Fig. 4D).

### 3.6. Administration of DSS causes CDHF diet-induced early tumorigenesis

Tumorigenesis was evaluated based on histological observations of the removed livers. On Day 35, no liver tumors were identified in either group. On Day 120, liver tumors were not identified in the 7 animals in the CDHF group, but they were found in 5 of the 10 animals in the CDHF+DSS group. In the 5 animals with liver tumors, 1 animal had 1 tumor, 3 animals had 2 tumors, and 1 animal had 3 tumors. The liver tumors ranged in size from 1.5 to 3.8 mm and had a mean size of 2.4 mm.

### 3.7. Correspondence of ultrasound findings with histopathological findings

The correlation of the HEC ratio to regions of fatty deposition is shown in Fig. 5A. Spearman's rank correlation coefficient was 0.3583 ($p = 0.0183$), indicating a significant correlation. The correlation of the HOLP index to sirius red-positive regions is shown in Fig. 5B. The correlation coefficient was −0.2238 ($p = 0.1543$), with no significant correlation.

Seven of the 10 histologically confirmed tumors (70.0 %) were successfully imaged with US (Fig. 5C). The mean diameter of the imaged tumors was 2.2±0.7 mm, and it did not differ significantly from the mean diameter of the tumors that were not imaged (2.9±0.9 mm) ($p = 0.2017$). The 3 tumors not imaged with US were present on the back or margin of the liver.

## 4. Discussions

Although the etiology of NASH is not well understood, the two-hit hypothesis is widely accepted [10]. Factors often responsible for the first hit are obesity, hypertension, hyperglycemia, and diabetes mellitus.

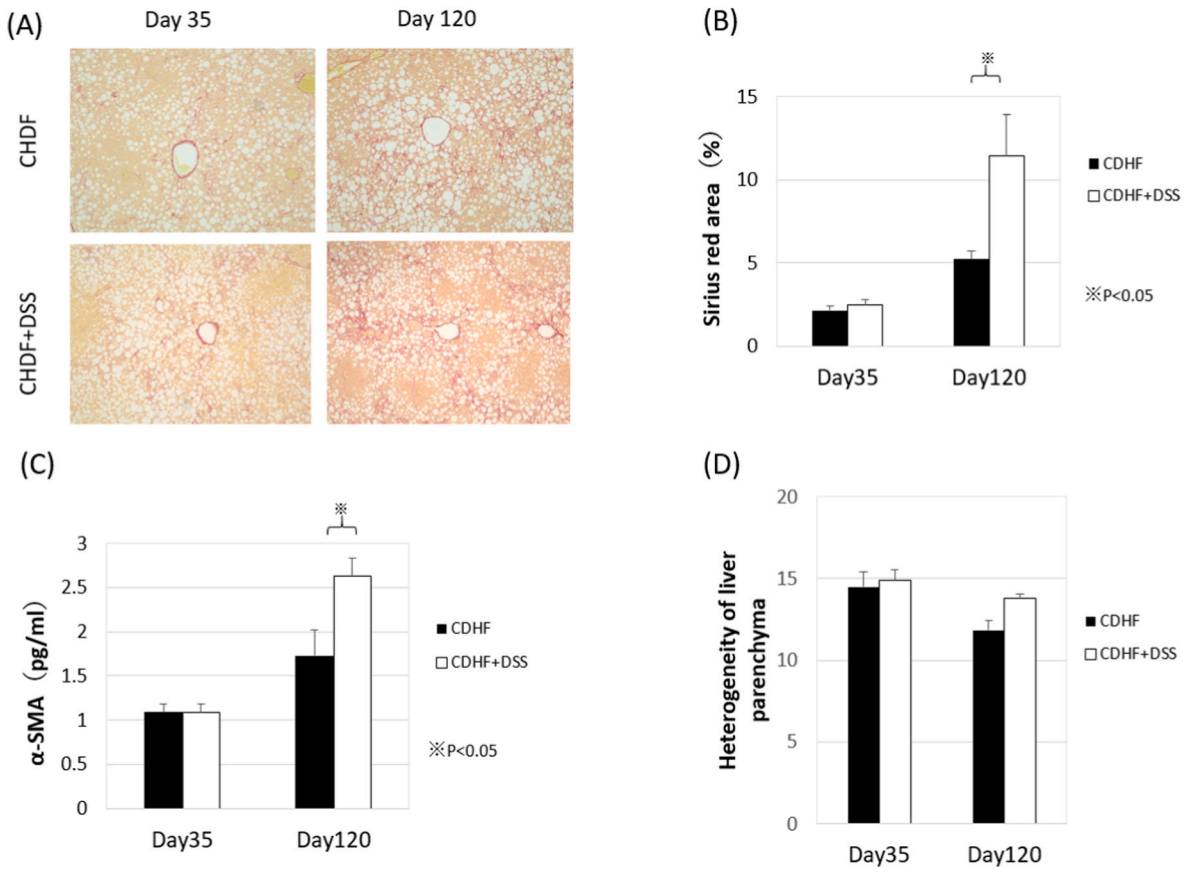


**Fig. 4.** Administration of DSS promotes CDHF diet-induced hepatic fibrosis
A: Sirius red-stained histopathological images of liver samples from necropsy on Days 35 and 120 ( × 100). Regions with fibrosis are stained red. B: Quantification of sirius red-positive areas on Days 35 and 120. Although the sirius red-positive area does not differ between the groups on Day 35, it is significantly larger in the CDHF+DSS group than in the CDHF group on Day 120. C: Mean levels of α-SMA on Days 35 and 120. Levels do not differ between the groups on Day 35, but are significantly higher in the CDHF+DSS group than in the CDHF group on Day 120. D: Mean heterogeneity of liver parenchyma on Days 35 and 120. Values do not differ between the groups on Day 35, but are higher in the CDHF+DSS group on Day 120, though not significantly. (For interpretation of the references to color in this figure legend, the reader is referred to the Web version of this article.)

On becoming steatotic, the liver is more susceptible to second hits from oxidative stress, iron deposition, endotoxins, mitochondrial dysfunction, lipid peroxidation, and inflammation-inducing cytokines [11–13].

Several animal models have been developed to study NAFLD and NASH. The following 3 feeding regimens are known to induce NAFLD or NASH in mice: methionine/choline-deficient (MCD), choline-deficient (CD), and high-fat (HF) diets. No diet, however, produces a complete model of human NASH. The MCD diet model has few long-term survivors, and weight loss is present. The CD diet model has only mild liver inflammation and fibrosis. Finally, the HF diet model has NAFLD, but no inflammation or fibrosis [14]. To resolve these shortcomings, a choline-deficient, high-fat (CDHF) diet combining the CD and HF diets was recently used to induce NASH. Cancer occurs in the resulting animal model with long-term observation [15].

In NAFLD and NASH, there are changes in the intestinal bacterial flora and increased intestinal permeability [1,16,17]. These conditions result in the entry of endotoxins into the liver via the portal vein, which exacerbates liver injury. This in turn stimulates Kupffer cells (liver--resident macrophages) [18]. Bacterial translocation occurring with the disruption of the barrier function of the colon then intensifies liver inflammation and fibrosis.

Recent studies have shown that disruption of the intestinal microbiome and endotoxin accumulation result in progressive hepatocyte proliferation, the expression of the hepatomitogen epiregulin, and apoptosis, which in turn promote the onset of hepatocellular carcinoma [19,20]. DSS is used to create a mouse model of ulcerative colitis [21,22]. Exposure of the large-intestinal mucosa to DSS via drinking water increases the permeability of the ileum and colon and brings about mucosal change [23,24]. Intestinal inflammation causes the release of inflammation-inducing cytokines from intestinal cells. These outcomes could be second hits in a model of hepatic steatosis.

Investigators familiar with the above background information created models of NASH by combining DSS in drinking water with a CDHF diet [8,25,26]. They used DSS in concentrations of 1 %–2 %. In a preliminary study we conducted, however, 6 of 15 mice fed a CDHF diet and given drinking water with 1 % DSS died over a 12-week observation period. Achiwa and colleagues reported the death of 5 of 16 mice treated under a similar protocol [8]. On the other hand, liver fibrosis and tumorigenesis at 12-week were not enough in 0.6%DSS in our pilot study.

In the present study, a protocol under which mice on a CDHF diet are given 0.8 % DSS in drinking water for 7 days followed by 10 days of MilliQ water was established. By the pilot study that preceded, Day35 was the time when hepatic steatosis were found clearly and in Day120, the advanced hepatic fibrosis and tumorigenesis were found.

Even with this lower 0.8 % concentration, the CDHF+DSS group had a significantly shorter long intestine and higher colonic histological score than the CDHF group on Days 35 and 120. IL-1β and IL-6 in large intestinal tissue reliably caused colitis.

On Days 35 and 120, inflammation of the liver parenchyma was serologically and histopathologically confirmed, and IL-1β expression was increased. Staining with F4/80 immunohistochemical stain, which

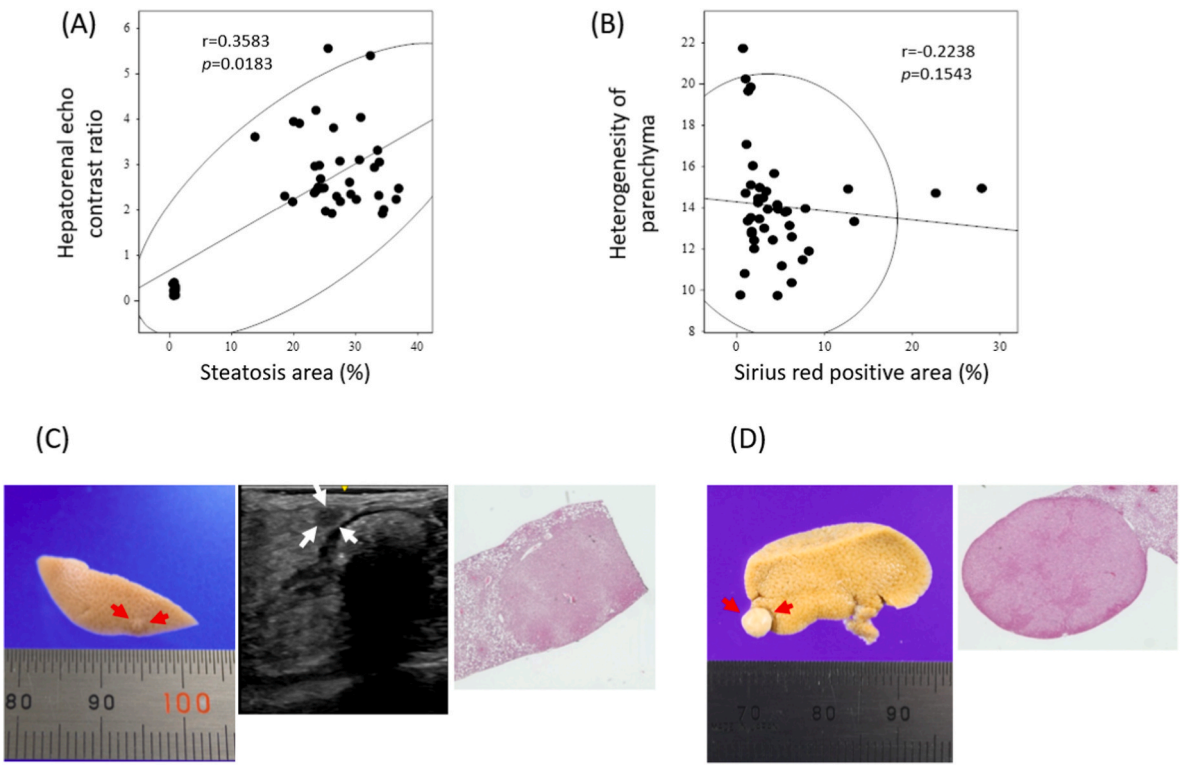


**Fig. 5.** Correspondence of ultrasound findings to histopathological findings
A: Correlation between the hepatorenal echo contrast ratio and steatosis area. Spearman's rank-correlation coefficient is 0.3583 ($P = 0.0183$), indicating a significant correlation. B: Correlation between the heterogeneity of liver parenchyma and the sirius red-positive area. The correlation coefficient is −0.2238 ($P = 0.1543$), showing no significant correlation.C: Macroscopic photograph of removed liver (left). A mass is identified (red arrows). This mass is also imaged on abdominal ultrasonography (center). Pathological examination shows mass formation (H&E, × 40) (right). D: A developing mass protruding from the margin of a removed liver (left, red arrows). Pathological examination shows the mass to be a liver tumor (right). This tumor is not imaged on abdominal ultrasonography. (For interpretation of the references to color in this figure legend, the reader is referred to the Web version of this article.)

shows inflammatory macrophage activation, resulted in a higher positive area in the CDHF+DSS group, indicating that disruption of the large-intestinal mucosal barrier function contributed to liver inflammation. Evaluations of fibrosis showed a larger sirius red-positive area and higher α-SMA expression in the CDHF+DSS group on Day 120. Five of the 10 animals in the CDHF+DSS group (50 %) and no animal in the CDHF group had a liver tumor on Day 120.

We conclude that a CDHF diet with intermittent 0.8 % DSS in the drinking water results in a stable, low-mortality model of NASH. This model begins exhibiting hepatic steatosis with inflammation by Day 35, with subsequent fibrosis and then tumor formation in 50 % of the animals by Day 120.

In conventional mouse models of NASH, fatty degeneration, fibrosis, and tumorigenesis in the liver are only evident on necropsy-based histological evaluation. The present study was performed with the conviction that these conditions could be identified with abdominal US.

B-mode US used in clinical settings is an invaluable tool for diagnosing hepatic steatosis based on findings including increased hepatic echogenicity [27], positive liver-kidney contrast [28], deep ultrasound attenuation in the liver [29], and poor or no visualization of intrahepatic vessels [30]. The present study focused on positive liver-kidney contrast, using HEC as a measure of fatty degeneration of the liver. Image analysis software was used to facilitate the objective evaluation of images. Concentration characteristics of the liver and kidneys were measured, and brightness was quantified. The ratio of brightness in the liver to the kidneys was defined as the HEC ratio. As seen in Fig. 5A, Spearman's rank-correlation coefficient of the HEC ratio and the area of histological fatty deposition was 0.3583, indicating a significant correlation ($P = 0.0183$).

Assessments on B-mode US of liver fibrosis are made according to differences in speckled patterns seen in the liver. Although this speckled pattern changes according to the wavenumber and shape of the outgoing ultrasound beam, it can also change according to the structure of the biological tissue in question and the properties of the tissues that include fibrosis [31]. Given that no procedure for quantifying speckled patterns has been established, the liver was selected as the ROI, concentration characteristics were measured, the standard deviation of brightness was calculated, and the results were defined as the HOLP index, using this index as a measure of liver fibrosis. However, as shown in Fig. 5B, there was, unfortunately, no correlation between the HOLP index and the area of histological fibrosis.

Transient elastography [7] and shear wave elastography (SWE) [5,32] have recently been developed as useful US procedures for diagnosing hepatic fibrosis. SWE was used to evaluate hepatic fibrosis by Morin and colleagues in a rat model of NASH in 2021 [33] and by Futani and colleagues in a mouse model of NASH in 2022 [34]. SWE, however, is available only on extremely expensive ultrasound machines. A new procedure is needed that can be used on inexpensive ultrasound machines commonly used in clinical practice, such as the machine used in the present study.

Xu and colleagues reported successfully imaging liver tumors in 18 of 20 nude mice (90.0 %) engrafted with hepatocellular carcinoma [35]. Tumor imaging performance in the present study was lower, at 70 %. One reason for this difference may be that the mean diameter of the liver tumors imaged by Xu and colleagues was 4.2 mm, which was larger than the mean diameter of 2.4 mm in the present study. In the present study, all tumors within the liver were imaged by US. The tumors not imaged were present at the margin of the liver or protruded from the liver on the back side.

The present study has shown that abdominal US can be used to assess

the degree of fatty degeneration and check for tumorigenesis in the liver in a mouse model of NASH. We are convinced, from an animal welfare perspective, that using abdominal US in mouse models of NASH would help reduce the number of animals that have to be killed unnecessarily.

### 4.1. Limitations

First, we did not use a healthy control group in this study. The comparison with the healthy control group would make it easy to understand results of this study.

Second, an evaluation of the cellular infiltration by the hematoxylin and eosin stain is not carried out objectively. Immunohistological staining method should have been used for these evaluations.

Third, the ultrasound device which we used in this study was only one model. Multiple models should have been tried for the setting of the optimal observation condition.

## 5. Conclusions

A stable, low-mortality model of NASH was established by feeding mice a CDHF diet with intermittent 0.8 % DSS in the drinking water. This model begins exhibiting hepatic steatosis with inflammation by Day 35, with subsequent fibrosis and then tumor formation in 50 % of the animals by Day 120.

Abdominal US can be used to assess the degree of fatty degeneration and check for tumorigenesis in the liver without the need for necropsy. This assessment procedure will reduce the number of mice killed unnecessarily during experiments, thereby contributing to animal welfare. In addition, the authors think that further experimental controls are required to support our conclusion.

## Funding

This work did not receive any grants from funding agencies in the public, commercial, or not-for-profit sectors.

## Declaration of competing interest

The authors declare that they have no known competing financial interests or personal relationships that could have appeared to influence the work reported in this paper.

## Acknowledgments

The authors would like to thank H. Tanaka and Y. Eda of the Research Center for Laboratory Animals, Dokkyo Medical University, Saitama Branch; K. Fukuda and F. Takei of the Collaborative Research Center, Dokkyo Medical University, Saitama Medical Center; and M. Nakayama of the Sankyo Labo Service Corporation, Inc., for technical assistance with the experiments.

## References

[1] L. Miele, V. Valenza, G. La Torre, M. Montalto, G. Cammarota, R. Ricci, R. Mascianà, A. Forgione, M.L. Gabrieli, G. Perotti, F.M. Vecchio, G. Rapaccini, G. Gasbarrini, C.P. Day, A. Grieco, Increased intestinal permeability and tight junction alterations in nonalcoholic fatty liver disease, Hepatology (Baltimore, Md 49 (2009) 1877–1887.

[2] Z.M. Younossi, A.B. Koenig, D. Abdelatif, Y. Fazel, L. Henry, M. Wymer, Global epidemiology of nonalcoholic fatty liver disease-Meta-analytic assessment of prevalence, incidence, and outcomes, Hepatology (Baltimore, Md 64 (2016) 73–84.

[3] T. Ito, M. Ishigami, B. Zou, T. Tanaka, H. Takahashi, M. Kurosaki, M. Maeda, K. N. Thin, K. Tanaka, Y. Takahashi, Y. Itoh, K. Oniki, Y. Seko, J. Saruwatari, M. Kawanaka, M. Atsukawa, H. Hyogo, M. Ono, E. Ogawa, S.D. Barnett, C.D. Stave, R.C. Cheung, M. Fujishiro, Y. Eguchi, H. Toyoda, M.H. Nguyen, The epidemiology of NAFLD and lean NAFLD in Japan: a meta-analysis with individual and forecasting analysis, 1995-2040, Hepatology Int. 15 (2021) 366–379.

[4] D.J.H. Tan, C.H. Ng, S.Y. Lin, X.H. Pan, P. Tay, W.H. Lim, M. Teng, N. Syn, G. Lim, J.N. Yong, J. Quek, J. Xiao, Y.Y. Dan, M.S. Siddiqui, A.J. Sanyal, M.D. Muthiah, R. Loomba, D.Q. Huang, Clinical characteristics, surveillance, treatment allocation, and outcomes of non-alcoholic fatty liver disease-related hepatocellular carcinoma: a systematic review and meta-analysis, the Lancet, Oncology 23 (2022) 521–530.

[5] T. Suda, O. Okawa, R. Masaoka, Y. Gyotoku, N. Tokutomi, Y. Katayama, M. Tamano, Shear wave elastography in hepatitis C patients before and after antiviral therapy, World J. Hepatol. 9 (2017) 64–68.

[6] T. Akima, M. Tamano, H. Hiraishi, Liver stiffness measured by transient elastography is a predictor of hepatocellular carcinoma development in viral hepatitis, Hepatol. Res. 41 (2011) 965–970.

[7] M. Yoneda, K. Fujita, M. Inamori, M. Tamano, H. Hiriishi, A. Nakajima, Transient elastography in patients with non-alcoholic fatty liver disease (NAFLD), Gut 56 (2007) 1330–1331.

[8] K. Achiwa, M. Ishigami, Y. Ishizu, T. Kuzuya, T. Honda, K. Hayashi, Y. Hirooka, Y. Katano, H. Goto, DSS colitis promotes tumorigenesis and fibrogenesis in a choline-deficient high-fat diet-induced NASH mouse model, Biochem. Biophys. Res. Commun. 470 (2016) 15–21.

[9] C. Bauer, P. Duewell, C. Mayer, H.A. Lehr, K.A. Fitzgerald, M. Dauer, J. Tschopp, S. Endres, E. Latz, M. Schnurr, Colitis induced in mice with dextran sulfate sodium (DSS) is mediated by the NLRP3 inflammasome, Gut 59 (2010) 1192–1199.

[10] C.P. Day, O.F. James, Steatohepatitis: a tale of two "hits"? Gastroenterology 114 (1998) 842–845.

[11] J.C. Cohen, J.D. Horton, H.H. Hobbs, Human fatty liver disease: old questions and new insights, Science (New York, N.Y.) 332 (2011) 1519–1523.

[12] T. Caballero, A. Gila, G. Sánchez-Salgado, P. Muñoz de Rueda, J. León, S. Delgado, J.A. Muñoz, M. Caba-Molina, A. Carazo, A. Ruiz-Extremera, J. Salmerón, Histological and immunohistochemical assessment of liver biopsies in morbidly obese patients, Histol. Histopathol. 27 (2012) 459–466.

[13] F. Caballero, A. Fernández, A.M. De Lacy, J.C. Fernández-Checa, J. Caballería, C. García-Ruiz, Enhanced free cholesterol, SREBP-2 and StAR expression in human NASH, J. Hepatol. 50 (2009) 789–796.

[14] L. Hebbard, J. George, Animal models of nonalcoholic fatty liver disease, Nat. Rev. Gastroenterol. Hepatol. 8 (2011) 35–44.

[15] M.J. Wolf, A. Adili, K. Piotrowitz, Z. Abdullah, Y. Boege, K. Stemmer, M. Ringelhan, N. Simonavicius, M. Egger, D. Wohlleber, A. Lorentzen, C. Einer, S. Schulz, T. Clavel, U. Protzer, C. Thiele, H. Zischka, H. Moch, M. Tschöp, A. V. Tumanov, D. Haller, K. Unger, M. Karin, M. Kopf, P. Knolle, A. Weber, M. Heikenwalder, Metabolic activation of intrahepatic CD8+ T cells and NKT cells causes nonalcoholic steatohepatitis and liver cancer via cross-talk with hepatocytes, Cancer Cell 26 (2014) 549–564.

[16] P. Brun, I. Castagliuolo, V. Di Leo, A. Buda, M. Pinzani, G. Palù, D. Martines, Increased intestinal permeability in obese mice: new evidence in the pathogenesis of nonalcoholic steatohepatitis, Am. J. Physiol. Gastrointest. Liver Physiol. 292 (2007) G518–G525.

[17] V. Volynets, M.A. Küper, S. Strahl, I.B. Maier, A. Spruss, S. Wagnerberger, A. Königsrainer, S.C. Bischoff, I. Bergheim, Nutrition, intestinal permeability, and blood ethanol levels are altered in patients with nonalcoholic fatty liver disease (NAFLD), Dig. Dis. Sci. 57 (2012) 1932–1941.

[18] K.C. El Kasmi, A.L. Anderson, M.W. Devereaux, S.A. Fillon, J.K. Harris, M.A. Lovell, M.J. Finegold, R.J. Sokol, Toll-like receptor 4-dependent Kupffer cell activation and liver injury in a novel mouse model of parenteral nutrition and intestinal injury, Hepatology (Baltimore, Md 55 (2012) 1518–1528.

[19] D.H. Dapito, A. Mencin, G.Y. Gwak, J.P. Pradere, M.K. Jang, I. Mederacke, J. M. Caviglia, H. Khiabanian, A. Adeyemi, R. Bataller, J.H. Lefkowitch, M. Bower, R. Friedman, R.B. Sartor, R. Rabadan, R.F. Schwabe, Promotion of hepatocellular carcinoma by the intestinal microbiota and TLR4, Cancer Cell 21 (2012) 504–516.

[20] E.J. Park, J.H. Lee, G.Y. Yu, G. He, S.R. Ali, R.G. Holzer, C.H. Osterreicher, H. Takahashi, M. Karin, Dietary and genetic obesity promote liver inflammation and tumorigenesis by enhancing IL-6 and TNF expression, Cell 140 (2010) 197–208.

[21] F. Obermeier, N. Dunger, U.G. Strauch, C. Hofmann, A. Bleich, N. Grunwald, H. J. Hedrich, E. Aschenbrenner, B. Schlegelberger, G. Rogler, J. Schölmerich, W. Falk, CpG motifs of bacterial DNA essentially contribute to the perpetuation of chronic intestinal inflammation, Gastroenterology 129 (2005) 913–927.

[22] I. Okayasu, S. Hatakeyama, M. Yamada, T. Ohkusa, Y. Inagaki, R. Nakaya, A novel method in the induction of reliable experimental acute and chronic ulcerative colitis in mice, Gastroenterology 98 (1990) 694–702.

[23] S. Melgar, A. Karlsson, E. Michaëlsson, Acute colitis induced by dextran sulfate sodium progresses to chronicity in C57BL/6 but not in BALB/c mice: correlation between symptoms and inflammation, Am. J. Physiol. Gastrointest. Liver Physiol. 288 (2005) G1328–G1338.

[24] P.A. Dawson, S. Huxley, B. Gardiner, T. Tran, J.L. McAuley, S. Grimmond, M. A. McGuckin, D. Markovich, Reduced mucin sulfonation and impaired intestinal barrier function in the hyposulfataemic NaS1 null mouse, Gut 58 (2009) 910–919.

[25] E. Gäbele, K. Dostert, C. Hofmann, R. Wiest, J. Schölmerich, C. Hellerbrand, F. Obermeier, DSS induced colitis increases portal LPS levels and enhances hepatic inflammation and fibrogenesis in experimental NASH, J. Hepatol. 55 (2011) 1391–1399.

[26] M.Y. Wang, Z.X. Wang, L.J. Huang, R.X. Yang, Z.Y. Zou, W.S. Ge, T.Y. Ren, J. G. Fan, Premorbid steatohepatitis increases the seriousness of dextran sulfate sodium-induced ulcerative colitis in mice, J. Clin. Translation. Hepatol. 10 (2022) 847–859.

[27] A.E. Joseph, K.C. Dewbury, P.G. McGuire, Ultrasound in the detection of chronic liver disease (the "bright liver"), Br. J. Radiol. 52 (1979) 184–188.

[28] Y. Yajima, K. Ohta, T. Narui, R. Abe, H. Suzuki, M. Ohtsuki, Ultrasonographical diagnosis of fatty liver: significance of the liver-kidney contrast, Tohoku J. Exp. Med. 139 (1983) 43–50.

[29] M. Hamaguchi, T. Kojima, Y. Itoh, Y. Harano, K. Fujii, T. Nakajima, T. Kato, N. Takeda, J. Okuda, K. Ida, Y. Kawahito, T. Yoshikawa, T. Okanoue, The severity of ultrasonographic findings in nonalcoholic fatty liver disease reflects the metabolic syndrome and visceral fat accumulation, Am. J. Gastroenterol. 102 (2007) 2708–2715.

[30] S. Saadeh, Z.M. Younossi, E.M. Remer, T. Gramlich, J.P. Ong, M. Hurley, K. D. Mullen, J.N. Cooper, M.J. Sheridan, The utility of radiological imaging in nonalcoholic fatty liver disease, Gastroenterology 123 (2002) 745–750.

[31] H. Toyoda, T. Kumada, N. Kamiyama, K. Shiraki, K. Takase, T. Yamaguchi, H. Hachiya, B-mode ultrasound with algorithm based on statistical analysis of signals: evaluation of liver fibrosis in patients with chronic hepatitis C, Ajr. Am. J. Roentgenol. 193 (2009) 1037–1043.

[32] Y. Gyotoku, R. Shirahashi, T. Suda, M. Tamano, Role of liver stiffness measurements in patients who develop hepatocellular carcinoma after clearance of the hepatitis C virus, J. Med. Ultrason. 49 (2022) (2001) 253–259.

[33] J. Morin, T.A. Swanson, A. Rinaldi, M. Boucher, T. Ross, D. Hirenallur-Shanthappa, Application of ultrasound and shear wave elastography imaging in a rat model of NAFLD/NASH, J. Vis. Exp. 170 (2021), e62403.

[34] F. Y, H. M, M. R, H. S, N. R, U. M, A. N, F. H, O. M, M. E, S. S, K. Y, Shear-wave elastography using commercially available ultrasound in a mouse model of chronic liver disease, Gastroontest. Disord. 4 (2022) 153–164.

[35] Z.T. Xu, H. Ding, T.T. Fu, Y.L. Zhu, W.P. Wang, A nude mouse model of orthotopic liver transplantation of human hepatocellular carcinoma HCCLM3 cell xenografts and the use of imaging to evaluate tumor progression, Med. Sci. Mon. Int. Med. J. Exp. Clin. Res. : Int. Med. J. Exp. Clin. Res. 25 (2019) 8694–8703.